Periodic potential can enormously boost free-particle transport induced by active fluctuations

K. Białas, J. Łuczka, and J. Spiechowicz*
Institute of Physics, University of Silesia, 41-500 Chorzów, Poland

(Received 4 July 2022; accepted 20 January 2023; published 7 February 2023)

Active fluctuations are detected in a growing number of systems due to self-propulsion mechanisms or collisions with an active environment. They drive the system far from equilibrium and can induce phenomena that are forbidden at equilibrium states by, e.g., fluctuation-dissipation relations and detailed balance symmetry. Understanding their role in living matter is emerging as a challenge for physics. Here we demonstrate a paradoxical effect in which a free-particle transport induced by *active fluctuations* can be boosted by many orders of magnitude when the particle is additionally subjected to a periodic potential. In contrast, within the realm of only *thermal fluctuations*, the velocity of a free particle exposed to a bias is reduced when the periodic potential is switched on. The presented mechanism is significant for understanding nonequilibrium environments such as living cells, where it can explain from a fundamental point of view why spatially periodic structures known as microtubules are necessary to generate impressively effective intracellular transport. Our findings can be readily corroborated experimentally, e.g., in a setup comprising a colloidal particle in an optically generated periodic potential.

DOI: 10.1103/PhysRevE.107.024107

I. INTRODUCTION

Microscopic systems are inherently immersed in a sea of thermal fluctuations that may strongly influence their properties or even induce an entirely new phenomenology. Celebrated examples include stochastic [1,2] or coherence [3,4] resonance, anomalous diffusion [5–7], ratchet effects [8–10], negative mobility [11–14], or thermal noise-induced dynamical localization [15,16], to name only a few. Nevertheless, the impact of thermal equilibrium fluctuations is limited by fundamental laws of nature, such as the fluctuation-dissipation theorem [17,18] or detailed balance symmetry [19,20].

These restrictions are no longer true for a nonequilibrium environment that keeps the system permanently out of thermal equilibrium even in the absence of external perturbations. A prototypical example are active fluctuations manifesting themselves either in (i) active matter harvesting energy from the environment into a self-propulsion drive [9,19,21–24], or (ii) an active bath such as a suspension of active colloids or swimming micro-organisms (e.g., *Escherichia coli*) pushing around a passive system [24–28]. Their relevance in biological systems is emerging as a hot topic that is a focus of researchers across all branches of natural science [29]. For instance, the latest experimental results make it clear that active fluctuations in living cells, generated by using energy derived from metabolic activities, are not just noise but are utilized to promote various physiological processes. In particular, biological motors such as kinesin or dynein benefit from active fluctuations and enhance their directional movement [30,31].

Within the realm of *thermal equilibrium fluctuations*, the directed velocity of a free particle exposed to a bias is usually reduced or at best conserved when an additional periodic potential is switched on [32]. Similarly, the diffusion coefficient D_0 of a free Brownian particle subjected to a periodic force is reduced to its effective diffusion constant $D < D_0$ [33,34]. In this work, we demonstrate a striking case that is the exact opposite, i.e., the particle can harness *active nonequilibrium fluctuations* to exploit an unbiased periodic potential and enhance its directed velocity much larger than for free transport. We identify its origin in the nature of active fluctuations, which, unlike thermal fluctuations, are not constrained by the equilibrium state, and therefore they may optimize themselves to make use of a periodic potential.

Our results are significant for understanding nonequilibrium environments and addressing important theoretical questions concerning the thermodynamics of active systems such as molecular motors inside living cells. They can be corroborated experimentally in a setup comprising a colloidal particle in an optically generated periodic potential [35,36] or a tested for real biological motors [30,31]. Moreover, they may open new avenues for designing ultrafast and efficient microscale and nanoscale machines.

The paper is organized as follows. In the next section we discuss the details of the studied model. In Sec. III we present the results. First, we show a paradoxical effect in which the periodic structure not only does not hinder the directed velocity of the particle, but it is involved in inducing the giant transport, which can be orders of magnitude greater than the velocity of the free particle. Second, we outline the mechanism of this phenomenon. Third, we discuss the role of symmetry breaking of the periodic potential and active fluctuations symmetry. The last section provides a summary and conclusions. In Appendix A we introduce the dimensionless units, while in Appendix B we detail the parametrization of the amplitude distribution of active fluctuations. In the final Appendix we display exemplary realizations of active fluctuations.

*jakub.spiechowicz@us.edu.pl

II. MODEL

We start our considerations with the overdamped motion of a free particle subjected to both active nonequilibrium fluctuations $\eta(t)$ and thermal noise $\xi(t)$,

$$\dot{x} = \eta(t) + \sqrt{2D_T}\,\xi(t), \tag{1}$$

where the dot denotes differentiation with respect to the time t. Thermal fluctuations $\xi(t)$ of temperature D_T are modeled by Gaussian white noise of zero mean $\langle \xi(t)\rangle = 0$ and the correlation function $\langle \xi(t)\xi(s)\rangle = \delta(t-s)$. Details of the scaling procedure are presented in Appendix A. We assume that $\langle \eta(t)\rangle = v_0 \neq 0$, and consequently active noise $\eta(t)$ induces the directed transport of the Brownian particle. Then one finds $\langle \dot{x}\rangle = v_0$. The essence of the proposed strategy for enhancement of the directed transport is to impose an unbiased periodic potential $U(x) = U(x+2\pi)$ on the system (1), i.e.,

$$\dot{x} = -\varepsilon U'(x) + \eta(t) + \sqrt{2D_T}\,\xi(t), \tag{2}$$

where ε is half of the potential barrier height, and the prime denotes differentiation with respect to the position x of the particle. First, we consider the simplest symmetric periodic potential,

$$U(x) = \sin x, \tag{3}$$

in order to avoid the apparent ratchet effect. Ratchet potentials that break the spatial symmetry should additionally enhance the free-particle transport and will be analyzed subsequently.

We ask for which model of active fluctuations $\eta(t)$ can the directed transport be enormously enhanced, i.e., $\langle \dot{x}\rangle \gg v_0$. As a candidate for $\eta(t)$ we choose Poisson white noise [37–39], which is a random sequence of δ-shaped pulses with random amplitudes z_i,

$$\eta(t) = \sum_{i=1}^{n(t)} z_i \delta(t - t_i), \tag{4}$$

where t_i are the arrival times of the Poisson counting process $n(t)$, i.e., the probability for the emergence of k impulses in the time interval $[0,t]$ is $\Pr\{n(t)=k\} = (\lambda t)^k \exp(-\lambda t)/k!$ [40]. The parameter λ is the mean number of δ-spikes per unit time (the firing rate of the Poisson process). The amplitudes $\{z_i\}$ of δ-kicks are statistically independent random variables sampled from the common probability distribution $\rho(z)$. The process $\eta(t)$ presents white noise of a finite mean and a covariance given by

$$\langle \eta(t)\rangle = \lambda\langle z_i\rangle, \quad \langle \eta(t)\eta(s)\rangle - \langle \eta(t)\rangle\langle \eta(s)\rangle = 2D_P\delta(t-s), \tag{5}$$

where $\langle z_i\rangle$ is an average over the amplitude distribution $\rho(z)$, and the noise intensity is $D_P = \lambda\langle z_i^2\rangle/2$. It is statistically symmetric if the density $\rho(z)$ is symmetric, i.e., when $\rho(z) = \rho(-z)$. In such a case, $\langle \eta(t)\rangle = 0$. However, we have to consider biased Poissonian noise for which $\langle \eta(t)\rangle = v_0 \neq 0$. Because there are infinitely many different statistics of the amplitudes $\{z_i\}$ for which $\langle \eta(t)\rangle = v_0$, we pick one of the most general forms of $\rho(z)$, namely the skew-normal distribution [41–44], which allows us to take into account both positive and negative amplitudes z_i as well as asymmetry in the distribution $\rho(z)$; cf. Appendix B. The skew-normal distribution is characterized by three independent parameters:

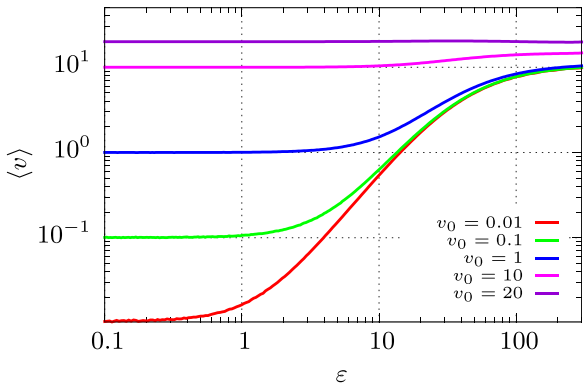

FIG. 1. The average velocity $\langle v\rangle$ of the Brownian particle dwelling in the symmetric potential $U(x) = \sin x$ and driven by active fluctuations $\eta(t)$ vs the potential barrier height ε for selected values of $\langle \eta(t)\rangle = v_0$. The parameters are as follows: the spiking rate $\lambda = 30$, the variance and skewness of the amplitude distribution $\rho(z)$ are $\sigma^2 = 3.1$ and $\chi = 0.99$, respectively, and the temperature is set to $D_T = 0.01$.

the mean value $\langle z_i\rangle = \zeta$, variance σ^2, and asymmetry (skewness) χ [45,46]. Active fluctuations $\eta(t)$ defined in this way are represented by white noise of average $\langle \eta(t)\rangle = \lambda\zeta$. We also assume that thermal and active fluctuations are uncorrelated, $\langle \xi(t)\eta(s)\rangle = \langle \xi(t)\rangle\langle \eta(s)\rangle = 0$. Noise $\eta(t)$ is applied in Ref. [47], and it can serve as a model for the stochastic release of energy in chemical reactions such as ATP hydrolysis or random collisions with complex and crowded environments. In this sense, our model is appropriate for both an active particle self-propelling itself inside a passive medium or a passive system immersed in an active bath formed as a suspension of active particles [28].

The main quantity of interest for the study of transport properties is the directed velocity defined as $\langle v\rangle = \lim_{t\to\infty}\langle x(t)\rangle/t$, where $\langle\cdot\rangle$ indicates the ensemble average. If $\eta(t) = 0$ in Eq. (2), then $\langle v\rangle = 0$. In the presence of active fluctuations with $\langle \eta(t)\rangle = v_0$, the free Brownian particle is transported with the average velocity $\langle v\rangle = v_0$. If under the identical experimental conditions the periodic potential $U(x)$ is turned on, one expects that the directed velocity will be notably reduced, $\langle v\rangle < v_0$, in particular for $U(x)$ with large barrier height ε [32].

III. RESULTS

Unfortunately, the Fokker-Planck-Kolmogorov-Feller integrodifferential equation corresponding to Eq. (2) cannot be solved analytically in a closed form [37]. Therefore, we resort to precise numerical simulations done by harvesting the GPU supercomputer using the CUDA environment [48]. The ensemble averaging was performed over Gaussian $\xi(t)$ and Poissonian $\eta(t)$ noise realizations [49] as well as over the initial conditions $x(0)$ distributed uniformly over the spatial period $[0, 2\pi]$ of the potential $U(x)$.

In Fig. 1 we present an effect that contradicts common intuition in which the periodic structure not only does not hinder the directed velocity of the particle, but it is involved in inducing the *giant transport*, which can be several orders

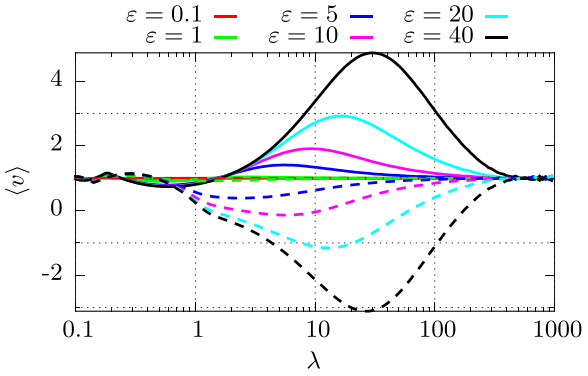

FIG. 2. The average velocity $\langle v\rangle$ vs the spiking rate λ of active fluctuations $\eta(t)$ for selected values of the potential barrier height ε and fixed $\langle\eta(t)\rangle = v_0 = 1$. Solid lines correspond to the asymmetry $\chi = 0.99$, whereas dashed lines correspond to $\chi = -0.99$. Other parameters are the variance $\sigma^2 = 3.1$ and temperature $D_T = 0.01$.

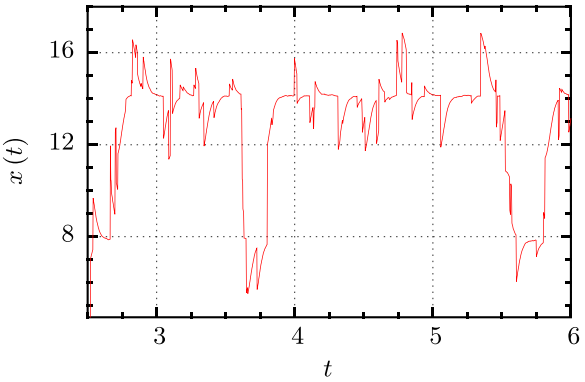

FIG. 3. Exemplary Brownian particle trajectory is shown for the potential barrier $\varepsilon = 40$. Other parameters are as follows: the spiking rate $\lambda = 30$, the average bias $\langle\eta(t)\rangle = v_0 = 1$, the variance $\sigma^2 = 3.1$, and the asymmetry $\chi = 0.99$ of the amplitude distribution $\rho(z)$. Temperature is fixed at $D_T = 0.01$.

of magnitude greater than the velocity of the free particle, i.e., $\langle v\rangle \gg v_0$. We note that when the barrier ε is increased, the average velocity $\langle v\rangle$ can be remarkably enhanced. For example, for $\langle\eta(t)\rangle = 0.01$ and $\varepsilon = 100$ the particle velocity reads $\langle v\rangle \approx 10 \gg v_0 = 0.01$, i.e., three orders of magnitude greater than for the free particle driven by the same active fluctuations $\eta(t)$. This giant transport behavior $\langle v\rangle \gg v_0$ is clearly induced by the additional presence of the symmetric periodic potential $U(x) = \sin x$ with deep wells. In Fig. 1 we show that amplification of $\langle v\rangle$ depends on v_0. For small $v_0 \ll 1$ the velocity $\langle v\rangle$ can be enormously boosted when the system is additionally subjected to a periodic potential $U(x)$. In such a case, $\langle v\rangle(\varepsilon)$ increases rapidly when ε grows. On the other hand, if the free-particle transport is already large, $v_0 \gg 1$, then there is no gain by placing the system in a periodic potential.

In many nonequilibrium systems, especially in living cells, there are no substantial systematic gradients or forces that could induce large transport. Instead one typically encounters unbiased or weakly biased fluctuations of both thermal and active (nonthermal) origin. Therefore, the presented mechanism might be crucial for a deep understanding of their physics. In Sec. III B we show that this nontrivial effect is heavily influenced by the statistics $\rho(z)$ of amplitudes z_i of fluctuations $\eta(t)$. In particular, it is not observed when z_i are distributed according to the frequently applied and even more asymmetric exponential probability density.

To explain the mechanism of this phenomenon, we first fix the mean of active fluctuations $\langle\eta(t)\rangle = 1$ and study how the velocity $\langle v\rangle$ depends on the spiking rate λ. This characteristic is depicted in Fig. 2. If $\lambda \to 0$ or $\lambda \to \infty$, then $\langle v\rangle \to v_0$. Since the bias of nonequilibrium noise is fixed, $\langle\eta(t)\rangle = \lambda\zeta = 1$, the average amplitude ζ of δ-spikes goes to infinity when $\lambda \to 0$ and therefore the potential $U(x)$ becomes negligible. On the other hand, when $\lambda \to \infty$ one stacks the infinite number of δ-kicks with vanishing mean, but the fixed variance $\sigma^2 = 3.1$ and the resultant movement mimics the free particle. The most striking feature of this panel is that for growing potential barrier ε there is the optimal spiking rate $\lambda_{\max}(\varepsilon)$ for which the velocity is maximal and significantly greater than the free-particle velocity $\langle v\rangle > v_0$. We stress that for smaller values of $\langle\eta(t)\rangle$ one observes the giant enhancement $\langle v\rangle \gg v_0$; cf. Fig. 1. The effect of ε-increase is twofold. First, it shifts the optimal $\lambda_{\max}(\varepsilon)$ towards larger values, and second, the magnitude of the velocity enhancement grows at $\lambda = \lambda_{\max}(\varepsilon)$.

In Fig. 2 one can also observe the impact of the asymmetry χ of the amplitude distribution $\rho(z)$; see Appendix B. At first glance it may seem that the transport direction is completely determined by the sign of the mean $\langle\eta(t)\rangle = \lambda\zeta$ of active fluctuations, which is controlled by the average value $\langle z_i\rangle = \zeta$ of δ-spikes distributed according to the probability density $\rho(z)$. However, this is not true in general. In particular, even though the statistical bias reads $\langle\eta(t)\rangle = v_0 = 1$, when χ is reversed from the positive $\chi = 0.99$ to the negative value $\chi = -0.99$ the transport direction is also inverted, i.e., $\langle v\rangle < 0$. Therefore, we conclude that in the studied case the orientation of the long tail in $\rho(z)$ is responsible for determining the direction of particle movement; cf. Appendix B. When the asymmetry is negative, the transport enhancement over the velocity of free particle $\langle v\rangle > v_0$ is still observed; however, its magnitude is a little bit smaller than for the situation when χ is positive.

In Fig. 3 we present the exemplary Brownian particle trajectory in the studied parameter regime with $\langle\eta(t)\rangle = 1$ and the large potential barrier $\varepsilon = 40$. Its careful inspection suggests that the occurring transport process may be decomposed onto two contributions. The first one is associated with the arrival of δ-kick, which is why the particle overcomes the potential barrier. In principle, in this way it can be carried over its many spatial periods. However, the second one, which is clearly missing for the free particle, is related to its relaxation towards the nearest potential minimum as it is, e.g., for $t \approx 2.6$ or $t \approx 5.6$. This contribution is at the root of the giant transport effect. When the mean value $\langle\eta(t)\rangle = v_0$ of active fluctuations is large, then regardless of the magnitude of the potential barrier ε, the particle velocity attains its free transport value $\langle v\rangle = v_0$; cf. Fig. 1. It is due to the fact that in such a limit the contribution coming from the relaxation is negligible. However, when $\langle\eta(t)\rangle = v_0$ is small [see, e.g., $\langle\eta(t)\rangle = v_0 = 0.01$ in Fig. 1], the sliding towards the potential

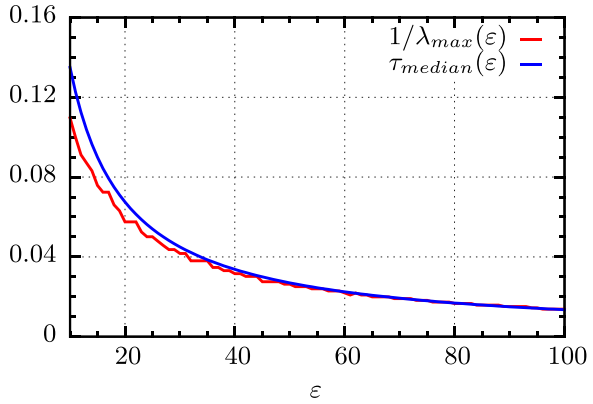

FIG. 4. The characteristic time $1/\lambda_{\max}(\varepsilon)$ between two successive δ-kicks of active fluctuations $\eta(t)$ and the estimated median time $\tau_{\text{median}}(\varepsilon)$ of particle relaxation towards the potential $U(x)$ minimum both as a function of the barrier height ε. Other parameters are as follows: the average value of active fluctuations $\langle\eta(t)\rangle = v_0 = 1$, variance $\sigma^2 = 3.1$, skewness $\chi = 0.99$ of the amplitude distribution $\rho(z)$, and temperature $D_T = 0.01$.

minima plays an essential role, and the giant transport occurs when the potential barrier ε is increased.

To illustrate this fact, we ask about the physical interpretation of the optimal spiking rate $\lambda_{\max}(\varepsilon)$ for which the rescaled particle velocity $\langle v\rangle/v_0$ assumes its maximal value when $\langle\eta(t)\rangle = v_0$ is fixed. In Fig. 4 we present the inverse of this characteristics $1/\lambda_{\max}(\varepsilon)$ and the estimated median time $\tau_{\text{median}}(\varepsilon)$ of particle relaxation towards the potential minimum both versus the barrier height ε. In the absence of all fluctuations, the latter relaxation for the potential $U(x) = \sin(x)$ with the barrier height ε is determined by the equation

$$\dot{x} = -\varepsilon U'(x) = -\varepsilon\cos x. \tag{6}$$

The time τ_{AB} at which the particle needs to move from point x_A to point x_B reads

$$\tau_{AB} = -\frac{1}{\varepsilon}\int_{x_A}^{x_B}\frac{dx}{\cos x} = -\frac{1}{2\varepsilon}\ln\left|\frac{1+\sin x}{1-\sin x}\right|\Bigg|_{x_A}^{x_B}. \tag{7}$$

After the arrival of the δ-spike, the particle can land at any random position x_A, and then during the time interval τ_{AB} it is relaxing towards the nearest potential minimum. This process ends at the random position x_B where another δ-spike of active nonequilibrium noise $\eta(t)$ emerges. As the potential is periodic, we restrict ourselves to the interval $x_A, x_B \in (\frac{\pi}{2}, \frac{3\pi}{2})$. Note that both the minimum and maximum are excluded because the time required to leave the maximum or reach the minimum is infinite, and Eq. (7) does not converge for these values. In Fig. 5 we present the relaxation time $|\tau_{AB}|$ for every pair of the starting and ending points taken from the considered interval $x_A, x_B \in (\frac{\pi}{2}, \frac{3\pi}{2})$. From this characteristic, the mean $\tau_{\text{mean}}(\varepsilon) \approx 1.72/\varepsilon$ and median $\tau_{\text{median}}(\varepsilon) \approx 1.35/\varepsilon$ of the relaxation time are evaluated.

In Fig. 4 one can clearly see that the initial discrepancy between these two characteristic timescales quickly dies out as ε is increased, and they become equivalent when the giant transport is detected. Such resonancelike behavior explains the mechanism of this counterintuitive effect. It means that the

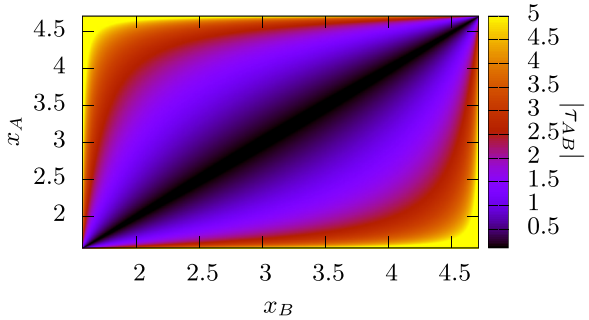

FIG. 5. Absolute value of the relaxation time $|\tau_{AB}|$ from the position x_A to x_B calculated according to Eq. (7).

enhancement of particle velocity over free transport is maximal when the average time $1/\lambda_{\max}(\varepsilon)$ between two successive δ-kicks of active fluctuations matches the interval $\tau_{\text{median}}(\varepsilon)$ needed for the particle to exploit the process of relaxation towards the potential minimum. The resulting motion is synchronized: the particle is δ-kicked and falls on one of the potential slopes, in the next time interval statistically there are no other δ-spikes and it relaxes to a neighboring minimum of the potential, and this scenario repeats over and over again. We now demonstrate that this mechanism is nontrivial and does not emerge, e.g., for the exponential distribution $\rho(z)$ of amplitudes z_i, which is even more asymmetric than the skew-normal distribution and arises in numerous different contexts.

A. Role of ratchet potentials

The next factor that can additionally boost the particle velocity is related to the potential symmetry. This issue is presented in Fig. 6 for three forms of the periodic potential: $U(x)$ is symmetric, whereas both $U_+(x)$ and $U_-(x)$ depict the asymmetric ratchet [50], and they read

$$U_+(x) = 0.908[\sin x + 0.25\sin(2x)], \tag{8a}$$

$$U_-(x) = 0.908[\sin x - 0.25\sin(2x)]. \tag{8b}$$

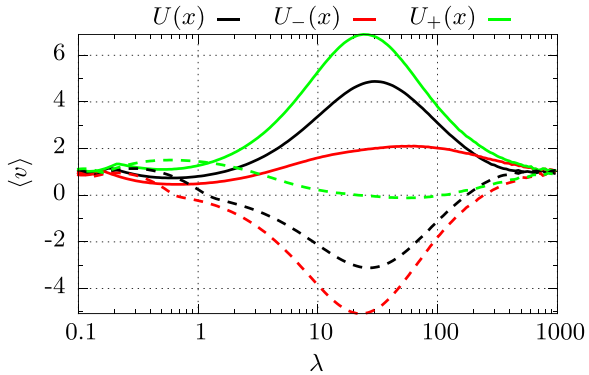

FIG. 6. Illustration of the role of potential symmetry on enhancement of free-particle transport. The potential barrier is $\varepsilon = 40$. The average bias $\langle\eta(t)\rangle = v_0 = 1$. Solid lines correspond to the asymmetry $\chi = 0.99$, whereas dashed lines correspond to $\chi = -0.99$. Other parameters are as follows: the variance $\sigma^2 = 3.1$, and temperature is fixed to $D_T = 0.01$.

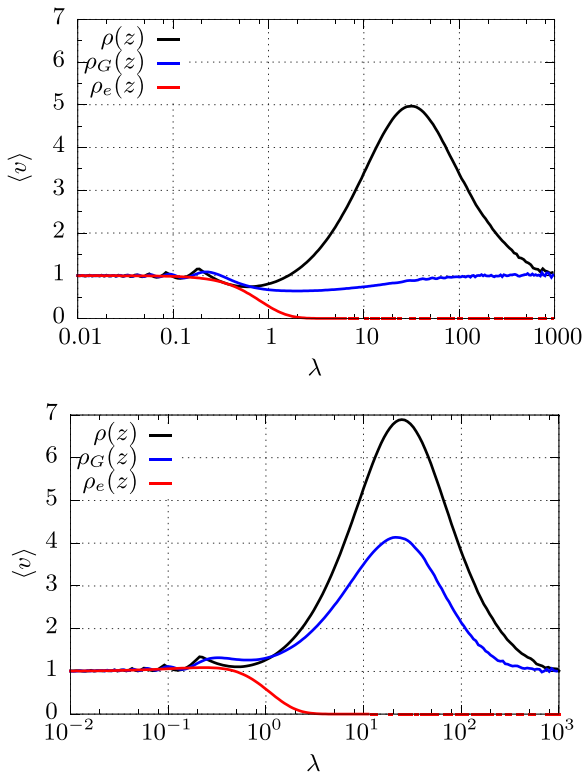

FIG. 7. The average velocity $\langle v\rangle$ vs the spiking rate λ of active fluctuations $\eta(t)$ depicted for three amplitude distributions and fixed $\langle\eta(t)\rangle = v_0 = \lambda\zeta = 1$, i.e., $\zeta = 1/\lambda$. $\rho(z)$ corresponds to the skew-normal statistics with $\sigma^2 = 3.1$ and $\chi = 0.99$; $\rho_G(z)$ indicates the Gaussian density with $\sigma^2 = 3.1$; $\rho_e(z)$ is the exponential distribution. The potential barrier height reads $\varepsilon = 40$, and temperature is fixed at $D_T = 0.01$. The upper panel corresponds to the symmetric potential $U(x)$, whereas in the bottom panel it is asymmetric, $U_+(x)$.

The prefactor 0.908 in $U_+(x)$ and $U_-(x)$ ensures that they possess the same barrier height as $U(x)$. The most important conclusion is that the giant increase of free transport depends on the particular realization of periodic substrates, and for an appropriate choice it can be amplified even further. For example, for the ratchet $U_+(x)$ the velocity $\langle v\rangle$ is noticeably larger than for the symmetric potential $U(x)$. By comparing these three potentials, one can notice that the distance between their maxima $x_{\max}$ and subsequent minima $x_{\min} > x_{\max}$ is greater for the ratchet $U_+(x)$ than for $U(x)$. Conversely, for $U_-(x)$ it is smaller than for $U(x)$. It is more likely that active fluctuations $\eta(t)$ will kick out the particle on the longer slope of the potential. Therefore, if $\chi = 0.99$ and the transport occurs in the positive direction, the velocity $\langle v\rangle$ for $U(x)$ is greater than for $U_-(x)$ and smaller than for $U_+(x)$. As we just explained, when $\chi = -0.99$ the particle moves in the negative direction and the situation is reversed.

B. Other statistics of amplitudes z_i

In Fig. 7 we present the average velocity $\langle v\rangle$ versus the spiking rate λ of active fluctuations $\eta(t)$ depicted for different amplitude distributions and fixed $\langle\eta(t)\rangle = v_0 = \lambda\zeta = 1$. We compare results obtained for active noise with the skew-normal statistics $\rho(z)$ to the case of Gaussian density $\rho_G(z)$ and the exponential distribution $\rho_e(z)$, namely

$$\rho_G(z) = \frac{1}{\sqrt{2\pi\sigma^2}} e^{-(z-\zeta)^2/2\sigma^2}, \quad \rho_e(z) = \theta(z)\zeta^{-1}e^{-z/\zeta}, \quad (9)$$

where $\theta(z)$ is the Heaviside step function. $\rho_G(z)$ is the symmetric distribution for which skewness reads $\chi = 0$, whereas the exponential statistics $\rho_e(z)$ with $\chi = 2$ is in fact even more asymmetric than the skew-normal density $\rho(z)$ with $\chi \in (-1, 1)$. In the upper panel of Fig. 7 we present the average velocity $\langle v\rangle$ as a function of spiking rate λ for the symmetric potential $U(x)$. In the bottom one the same characteristics is depicted but for the asymmetric (ratchet) substrate $U_+(x)$. Comparison of these two plots illustrates that potential asymmetry can additionally boost the free-particle transport. This result is in agreement with the insights presented in Fig. 6.

We can observe that the enormous boost for the free-particle transport induced by the periodic potential detected for $\lambda = \lambda_{\max} \sim \varepsilon$ is not rooted solely in the asymmetry (nonzero skewness) of active noise amplitude distribution since in both panels this effect is not present for the exponential statistics $\rho_e(z)$. In particular, the particle velocity $\langle v\rangle$ either tends to unity when $\lambda \to 0$ or vanishes if $\lambda \to \infty$. Moreover, when the periodic potential is asymmetric, cf. the bottom panel with $U_+(x)$, the transport enhancement $\langle v\rangle > v_0$ is discovered even for active noise with amplitudes distributed according to the symmetric Gaussian density $\rho_G(z)$. On the other hand, if the potential is symmetric, see the upper plot with $U(x)$, only active fluctuations with amplitudes drawn from the skew-normal distribution $\rho(z)$ result in the velocity amplification $\langle v\rangle > v_0$. The question about general constraints on the probability density for δ-spike amplitudes that allow for the emergence of the studied effect is complex and beyond the scope of the current paper. Here we only point out the important difference between the exponential and skew-normal statistics. In the former, all moments disappear when the mean vanishes $\zeta \to 0$, whereas in the latter, mean ζ, variance σ^2, and skewness are independent parameters. This means that even though $\zeta \to 0$, the variance and skewness can still be finite and fixed.

Our results reveal that periodic potentials can boost the free-particle transport driven by white Poissonian noise provided that (i) its amplitude distribution allows for both positive and negative δ-spikes, and (ii) the amplitude statistics possesses nonzero skewness or the reflection symmetry of the potential is broken. These are nontrivial conditions for the occurrence of this effect. The fact that active noise with fixed mean and both positive and negative amplitudes can induce significantly greater directed transport than for active noise of equal average but with only positive δ-spikes is in addition highly counterintuitive.

IV. DISCUSSION

The proposed strategy for the giant boost of free transport allows us to understand why sometimes the existence of periodic structures is beneficial for transport efficiency. Many transport processes in biological cells are driven by diffusion, and consequently their effectiveness is low. Therefore, cells have developed another mechanism of movement via micro-

tubules that are asymmetric periodic structures that provide platforms for intracellular transport mediated by molecular motors. These platforms can be formed rapidly in response to cellular needs. They have a half-life of 5–10 min [51] and typically are nucleated and organized by microtubule-organizing centers. The polarized structure of microtubules provides the navigational information necessary to direct cargo to the proper destination in the cell. A biological motor such as a conventional kinesin moves along a microtubule of period 8 nm with a directed velocity 1800 nm/s. Our conclusion is that as nature teaches us, transport within periodic structures can be many orders of magnitude more efficient than without it. Whether nature takes advantage of this possibility is another matter, of course.

In summary, we demonstrated a paradoxical effect in which the velocity of a free Brownian particle exposed to active fluctuations might be enormously accelerated when it is placed in a periodic potential. Its origin lies in the versatile nature of *active nonequilibrium fluctuations*, which allow them to fine-tune to the given substrate and transport the particle across the potential barrier, where it is able to effortlessly exploit its steepness. This phenomenon should be contrasted with the celebrated giant diffusion effect [52–55] in which *thermal equilibrium fluctuations* cooperate with a tilted periodic potential to accelerate diffusion of a particle by many orders of magnitude as compared to free thermal diffusion.

We considered a paradigmatic model of nonequilibrium statistical physics that comprises numerous realizations [32], and therefore we expect that our results will inspire vibrant follow-up work. Moreover, the findings may be corroborated experimentally in a dissipative optical environment in which the potential barrier can be easily tuned [35,36]. Our results carry impactful consequences not only for microscopic physical systems, but also biological ones such as molecular motors, which are *in situ* immersed in an unavoidable sea of thermal and active fluctuations. Finally, our results may open new avenues for designing ultrafast and efficient microscale and nanoscale machines.

ACKNOWLEDGMENTS

This work has been supported by the Grant NCN No. 2022/45/B/ST3/02619 (J.S.).

APPENDIX A: DIMENSIONLESS UNITS

Transforming the equation describing the model into its dimensionless form allows us to simplify the analysis because it can reduce the number of parameters appearing before such a procedure. Moreover, the resulting representation is independent of a specific experimental setup allowing us to choose the best platform for corroborating theoretical predictions. We start with the Langevin equation for an overdamped Brownian particle in a periodic potential $U(x)$ immersed in both an active $\eta(t)$ and a thermal $\xi(t)$ bath,

$$\Gamma\dot{x} = -E\,U'(x) + \eta(t) + \sqrt{2\Gamma k_B T}\,\xi(t), \tag{A1}$$

where Γ is the friction coefficient, E is half of the potential barrier height, k_B is the Boltzmann constant, and T denotes thermostat temperature. The potential is assumed in the periodic form

$$U(x) = U(x+L). \tag{A2}$$

We rescale the position and time in the following way:

$$\hat{x} = 2\pi\frac{x}{L}, \quad \hat{t} = \frac{t}{\tau_0},$$
$$\tau_0 = \frac{L}{100v_{D_0}} = \frac{L}{100D_0/L} = \frac{L^2}{100k_BT/\Gamma}, \tag{A3}$$

where v_{D_0} is the characteristic velocity corresponding to free thermal diffusion, $D_0 = k_BT/\Gamma$. The additional multiplier 100 is introduced in the denominator due to technical reasons outlined below. Under such a choice of the scales, Eq. (A1) becomes

$$\dot{\hat{x}} = -\varepsilon\hat{U}'(\hat{x}) + \hat{\eta}(\hat{t}) + \sqrt{2D_T}\,\hat{\xi}(\hat{t}), \tag{A4}$$

where the dimensionless barrier height is $\varepsilon = E/(100k_BT)$. The rescaled potential reads

$$\hat{U}(\hat{x}) = U\left(\frac{L}{2\pi}\hat{x}\right). \tag{A5}$$

For example, if $U(x) = \sin(2\pi x/L)$, then $\hat{U}(\hat{x}) = \sin\hat{x}$ possesses the spatial period 2π. The scaling procedure allows us to reduce a number of free parameters by

$$\gamma = 1, \quad D_T = 0.01. \tag{A6}$$

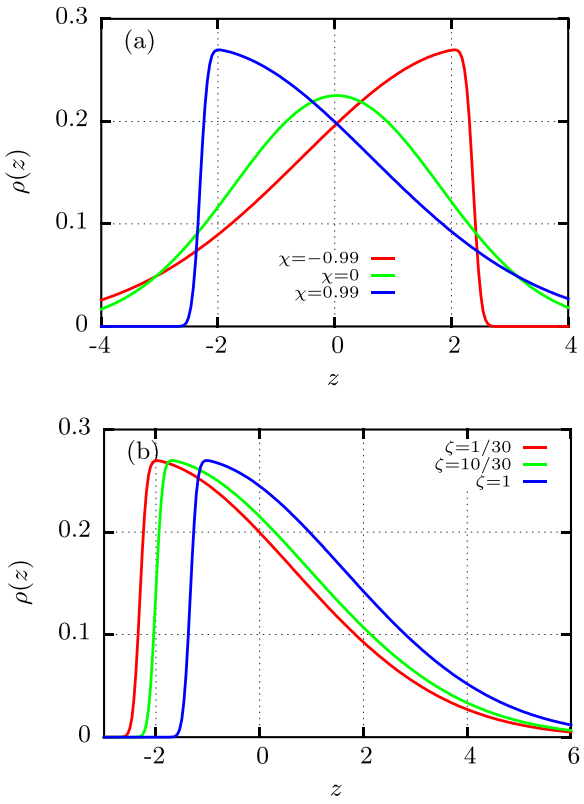

FIG. 8. The probability distribution $\rho(z)$ of amplitudes z_i of active nonequilibrium fluctuations $\eta(t)$ is presented in panel (a) for fixed mean $\zeta = 1/30$, variance $\sigma^2 = 3.1$, and different values of skewness χ, and in panel (b) for various mean ζ with skewness $\chi = 0.99$.

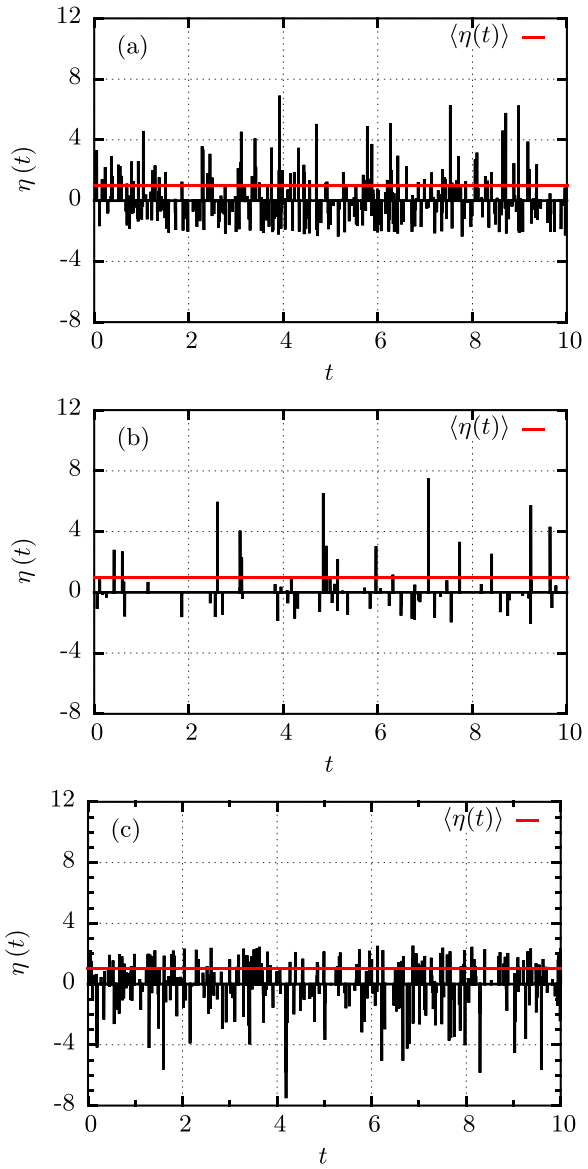

FIG. 9. Three exemplary realizations of active nonequilibrium noise $\eta(t)$ for different parameters: (a) $\lambda = 30$, $\zeta = 1/30$, $\sigma^2 = 3.1$, and $\chi = 0.99$; (b) $\lambda = 6$, $\zeta = 1/6$, $\sigma^2 = 3.1$, and $\chi = 0.99$; (c) $\lambda = 30$, $\zeta = 1/30$, $\sigma^2 = 3.1$, and $\chi = -0.99$. The solid red line corresponds to the average $\langle\eta(t)\rangle = 1$.

Dimensionless thermal noise

$$\hat{\xi}(\hat{t}) = \frac{L}{2\pi}\frac{1}{100k_BT}\xi(\tau_0\hat{t}). \tag{A7}$$

exhibits the same statistical properties as the dimensional one, i.e., it has the same vanishing mean and correlation function. The rescaled Poissonian shot noise becomes

$$\hat{\eta}(\hat{t}) = \frac{L}{2\pi}\frac{1}{100k_BT}\eta(\tau_0\hat{t}), \tag{A8}$$

and it is characterized by the dimensionless spiking rate

$$\hat{\lambda} = \tau_0\lambda. \tag{A9}$$

The error of the numerical integration scheme to solve stochastic differential equations driven by Poissonian white shot noise as well as the computation time increases significantly when the frequency $\hat{\lambda}$ of δ-kicks grows [56]. To reduce this drawback, we introduced the additional multiplier 100 in the definition of the characteristic timescale τ_0, which allows us to limit the range of spiking rate $\hat{\lambda}$ needed in this study. Because only dimensionless quantities are used in the main text, we omit the hat notation there.

APPENDIX B: PARAMETRIZATION OF AMPLITUDE DISTRIBUTION $\rho(z)$

The skew-normal distribution [42] is usually defined in terms of a location μ representing the shift, a scale ω proportional to the variance, and a parameter α describing the shape. The probability density function then reads

$$\rho(z) = \frac{2}{\sqrt{2\pi\omega^2}}e^{-\frac{(z-\mu)^2}{2\omega^2}}\int_{-\infty}^{\alpha[(z-\mu)/\omega]} ds\,\frac{1}{2\pi}e^{-\frac{s^2}{2}}. \tag{B1}$$

The quantities μ, ω, and α can be represented by more intuitive parameters, namely the mean $\mu \to \zeta = \langle z_i\rangle$, variance $\omega \to \sigma^2 = \langle(z_i - \langle z_i\rangle)^2\rangle$, and skewness $\alpha \to \chi = \langle[(z_i - \langle z_i\rangle)/\sigma]^3\rangle$ of the distribution $\rho(z)$. The average amplitude ζ allows for direct control of mean bias $\langle\eta(t)\rangle = v_0 = \lambda\zeta$ of nonequilibrium noise, the variance σ^2 describes the mean-square deviation of δ-spikes, and skewness χ measures the asymmetry of skew-normal distribution. Expressions for the location μ, scale ω, and shape α in terms of these parameters are as follows [45,46]:

$$\alpha = \frac{\delta}{\sqrt{1-\delta^2}}, \tag{B2a}$$

$$\omega = \sqrt{\frac{\sigma^2}{1-2\delta^2/\pi}}, \tag{B2b}$$

$$\mu = \zeta - \delta\sqrt{\frac{2\sigma^2}{\pi(1-2\delta^2/\pi)}}, \tag{B2c}$$

where δ is defined as

$$\delta = \mathrm{sgn}(\chi)\sqrt{\frac{|\chi|^{2/3}}{(2/\pi)\{[(4-\pi)/2]^{2/3} + |\chi|^{2/3}\}}}. \tag{B3}$$

In Fig. 8 we present the probability density function $\rho(z)$ for amplitudes of active nonequilibrium noise $\eta(t)$ as a function of its parameters, i.e., mean ζ, variance σ^2, and skewness χ. In panel (a) the impact of skewness χ for the fixed mean $\zeta = 1/30$ is shown, whereas in (b) the influence of mean ζ is illustrated for $\chi = 0.99$.

APPENDIX C: REALIZATIONS OF ACTIVE FLUCTUATIONS $\eta(t)$

In Fig. 9 we demonstrate three exemplary realizations of active nonequilibrium noise $\eta(t)$ for different values of its parameters. For all the presented cases the statistical bias is fixed to $\langle\eta(t)\rangle = v_0 = 1$. Panel (a) corresponds to the regime of optimal transport $\langle v\rangle$ for the potential barrier height $\varepsilon = 40$ (see Fig. 2 in the main text), the spiking rate $\lambda = 30$, mean amplitude $\zeta = 1/30$, variance $\sigma^2 = 3.1$, and skewness

$\chi = 0.99$. In panel (b) the frequency is five times smaller, $\lambda = 6$, and therefore $\zeta = 1/\lambda = 1/6$ to satisfy the condition $\langle \eta(t) \rangle = \lambda\zeta = v_0 = 1$. The reader can indeed infer that the parameter λ describes the frequency of δ-spikes, whereas an increase of ζ has a twofold effect: (i) the positive amplitudes $z_i > 0$ grow, and (ii) the negative ones $z_i < 0$ are reduced. Finally, in panel (c) we present the impact of skewness inversion $\chi \to -\chi$. As it is visualized in this plot, such an operation corresponds to reflection of the realization about the axis $\eta(t) = \zeta$.

[1] R. Benzi, A. Sutera, and A. Vulpiani, J. Phys. A **14**, L453 (1981).
[2] L. Gammaitoni, P. Hänggi, P. Jung, and F. Marchesoni, Rev. Mod. Phys. **70**, 223 (1998).
[3] A. S. Pikovsky and J. Kurths, Phys. Rev. Lett. **78**, 775 (1997).
[4] B. Lindner, J. Garcia-Ojalvo, A. Neiman, and L. Schimansky-Geier, Phys. Rep. **392**, 321 (2004).
[5] J. P. Bouchaud and A. Georges, Phys. Rep. **195**, 127 (1990).
[6] R. Metzler, J. H. Jeon, A. G. Cherstvy, and E. Barkai, Phys. Chem. Chem. Phys. **16**, 24128 (2014).
[7] J. Spiechowicz, P. Hänggi, and J. Łuczka, New J. Phys. **21**, 083029 (2019).
[8] P. Hänggi and F. Marchesoni, Rev. Mod. Phys. **81**, 387 (2009).
[9] C. J. O. Reichhardt and C. Reichhardt, Annu. Rev. Condens. Matter Phys. **8**, 51 (2017).
[10] J. Spiechowicz, J. Łuczka, and P. Hänggi, Sci. Rep. **6**, 30948 (2016).
[11] L. Machura, M. Kostur, P. Talkner, J. Łuczka, and P. Hänggi, Phys. Rev. Lett. **98**, 040601 (2007).
[12] D. Speer, R. Eichhorn, and P. Reimann, Phys. Rev. E **76**, 051110 (2007).
[13] J. Nagel, D. Speer, T. Gaber, A. Sterck, R. Eichhorn, P. Reimann, K. Ilin, M. Siegel, D. Koelle, and R. Kleiner, Phys. Rev. Lett. **100**, 217001 (2008).
[14] A. Słapik, J. Łuczka, P. Hänggi, and J. Spiechowicz, Phys. Rev. Lett. **122**, 070602 (2019).
[15] J. Spiechowicz and J. Łuczka, Sci. Rep. **7**, 16451 (2017).
[16] J. Spiechowicz and J. Łuczka, Chaos **29**, 013105 (2019).
[17] R. Kubo, Rep. Prog. Phys. **29**, 255 (1966).
[18] U. M. B. Marconi, A. Puglisi, L. Rondoni, and A. Vulpiani, Phys. Rep. **461**, 111 (2008).
[19] M. E. Cates, Rep. Prog. Phys. **75**, 042601 (2012).
[20] F. S. Gnesotto, F. Mura, J. Gladrow, and C. P. Broedersz, Rep. Prog. Phys. **81**, 066601 (2018).
[21] S. Ramaswamy, Annu. Rev. Condens. Matter Phys. **1**, 323 (2010).
[22] P. Romanczuk, M. Bar, W. Ebeling, B. Lindner, and L. Schimansky-Geier, Eur. Phys. J. Spec. Top. **202**, 1 (2012).
[23] M. C. Marchetti, J. F. Joanny, S. Ramaswamy, T. B. Liverpool, J. Prost, M. Rao, and R. A. Simha, Rev. Mod. Phys. **85**, 1143 (2013).
[24] C. Bechinger, R. Di Leonardo, H. Löwen, C. Reichhardt, G. Volpe, and G. Volpe, Rev. Mod. Phys. **88**, 045006 (2016).
[25] C. Maggi, M. Paoluzzi, N. Pellicciotta, A. Lepore, L. Angelani and R. Di Leonardo, Phys. Rev. Lett. **113**, 238303 (2014).
[26] K. Kanazawa, T. G. Sano, T. Sagawa, and H. Hayakawa, Phys. Rev. Lett. **114**, 090601 (2015).
[27] C. Maggi, M. Paoluzzi, L. Angelani and R. Di Leonardo, Sci. Rep. **7**, 17588 (2017).
[28] L. Dabelow, S. Bo, and R. Eichhorn, Phys. Rev. X **9**, 021009 (2019).
[29] K. Kanazawa, T. G. Sano, A. Cairoli, and A. Baule, Nature (London) **579**, 364 (2020).
[30] Y. Ezber, V. Belyy, S. Can, and A. Yildiz, Nat. Phys. **16**, 312 (2020).
[31] T. Ariga, K. Tateishi, M. Tomishige, and D. Mizuno, Phys. Rev. Lett. **127**, 178101 (2021).
[32] H. Risken, *The Fokker-Planck Equation: Methods of Solution and Applications* (Springer-Verlag, Berlin, 1996).
[33] S. Lifson and J. L. Jackson, J. Chem. Phys. **36**, 2410 (1962).
[34] R. Festa and E. Galleani d'Agliano, Physica A **90**, 229 (1978).
[35] J. T. Park, G. Paneru, Ch. Kwon, S. Granick, and H. K. Pak, Soft Matter **16**, 8122 (2020).
[36] G. Paneru, J. T. Park, and H. K. Pak, J. Phys. Chem. Lett. **12**, 11078 (2021).
[37] P. Hänggi, Z. Phys. B **30**, 85 (1978).
[38] J. Spiechowicz, P. Hänggi, and J. Łuczka, Phys. Rev. E **90**, 032104 (2014).
[39] K. Białas, J. Łuczka, P. Hänggi, and J. Spiechowicz, Phys. Rev. E **102**, 042121 (2020).
[40] W. Feller, *An Introduction to Probability Theory and Its Applications* (Wiley, New York, 1970).
[41] A. O'hagan and T. Leonard, Biometrika **63**, 201 (1976).
[42] A. Azzalini, Scand. J. Statist. **12**, 171 (1985).
[43] K. Rijal, A. Prasad, A. Singh, and D. Das, Phys. Rev. Lett. **128**, 048101 (2022).
[44] M. L. Bailey, H. Yan, I. Surovtsev, J. F. Williams, M. C. King, and S. G. J. Mochrie, Phys. Rev. E **103**, 032405 (2021).
[45] N. Henze, Scand. J. Statist. **13**, 271 (1986).
[46] D. Ghorbanzadeh, P. Durand, and L. Jaupi, Proc. World Congress Eng. **1**, 113 (2017).
[47] J. S. Lee and H. Park, Phys. Rev. E **105**, 024130 (2022).
[48] J. Spiechowicz, M. Kostur, and Ł. Machura, Comput. Phys. Commun. **191**, 140 (2015).
[49] P. Hänggi, Z. Phys. B **36**, 271 (1980).
[50] J. Łuczka, R. Bartussek, and P. Hänggi, Europhys. Lett. **31**, 431 (1995).
[51] A. S. Infante, M. S. Stein, Y. Zhai, G. G. Borisy, and G. G. Gundersen, J. Cell Sci. **113**, 3907 (2000).
[52] P. Reimann, C. Van den Broeck, H. Linke, P. Hänggi, J. M. Rubi, and A. Perez-Madrid, Phys. Rev. Lett. **87**, 010602 (2001).
[53] B. Lindner and I. M. Sokolov, Phys. Rev. E **93**, 042106 (2016).
[54] A. M. Berezhkovskii and L. Dagdug, J. Chem. Phys. **151**, 131102 (2019).
[55] J. Spiechowicz and J. Łuczka, Phys. Rev. E **104**, 034104 (2021).
[56] C. Kim, E. K. Lee, P. Hänggi, and P. Talkner, Phys. Rev. E **76**, 011109 (2007).